# SHEATH VOLTAGE RATIO FOR ASYMMETRIC RF DISCHARGES

by

M. V. Alves, M. A. Lieberman, V. Vahedi,
and C. K. Birdsall

Memorandum No. UCB/ERL M90/56

21 June 1990

# SHEATH VOLTAGE RATIO FOR ASYMMETRIC RF DISCHARGES

by

M. V. Alves, M. A. Lieberman, V. Vahedi,
and C. K. Birdsall

Memorandum No. UCB/ERL M90/56

21 June 1990

**ELECTRONICS RESEARCH LABORATORY**

College of Engineering
University of California, Berkeley
94720

# SHEATH VOLTAGE RATIO FOR ASYMMETRIC RF DISCHARGES

by

M. V. Alves, M. A. Lieberman, V. Vahedi,
and C. K. Birdsall

Memorandum No. UCB/ERL M90/56

21 June 1990

**ELECTRONICS RESEARCH LABORATORY**

College of Engineering
University of California, Berkeley
94720

# SHEATH VOLTAGE RATIO FOR ASYMMETRIC RF DISCHARGES

M. V. Alves[1], M. A. Lieberman,
V. Vahedi and C. K. Birdsall
Department of Electrical Engineering and Computer Sciences, and
the Electronics Research Laboratory
University of California, Berkeley, CA 94720

## ABSTRACT

Spherical and cylindrical many-particle models are used to simulate RF discharges in which the RF powered and the grounded electrodes have different areas. This asymmetry determines the magnitude of the average plasma-to-electrode voltage $V_a$ (the ion bombarding energy) at the smaller powered electrode, which is a critical process parameter. A collisionless uniform ionization discharge model predicts that the voltage ratio $V_a/V_b$ scales as the fourth power of the electrode area ratio $A_b/A_a$ where $V_b$ is the potential drop at the other electrode. However, measurements indicate a much weaker dependence of $V_a/V_b$ on the area ratio, which is also observed in our simulations. Over a limited range of area ratios it was found that the power dependence was close to one, in agreement with a local ionization discharge model. The codes are PDC1 and PDS1 (cylindrical and spherical, respectively), which utilize particle-in-cell techniques plus Monte-Carlo simulation of electron-neutral (elastic, excitation and ionization) and ion-neutral (scattering and charge-exchange) collisions.

---

1. Permanent address: INPE, P. O. Box 515, S. J. dos Campos, SP, 12201, Brazil.

## I. INTRODUCTION

Capacitive discharges are widely used for materials processing in the electronics industry. The discharges are generally asymmetric: the RF powered electrode and the grounded electrode have different areas, $A_a$ and $A_b$ respectively, with $A_a$ typically less than $A_b$. This asymmetry determines the magnitude of the plasma-to-electrode voltage $V_a$ (the ion bombarding energy) at the powered electrode, which is a critical parameter for VLSI processing. A simple collisionless discharge model[1] predicts the scaling $V_a/V_b = (A_b/A_a)^4$; however, measurements indicate a much weaker dependence of $V_a/V_b$ on the area ratio[2]. For capacitive discharges, almost all the voltage drop appears across thin sheaths, having thicknesses $s_a$ and $s_b$, at the powered and grounded electrodes. In most cases there is an external blocking capacitor, $C_B$, having negligible impedance at the RF driving frequency, in series with the driven electrode. Between the sheaths there is a thermal plasma or "glow" region with a thickness $d \geq s$ which serves to maintain the discharge by means of ion generation there, balancing loss of particles to the electrodes. These processes of ionization and loss determine the plasma density profile and, in particular, the densities $n_a$ and $n_b$ at the two sheath edges near the powered and grounded electrodes, which are found not to be equal as is often assumed. In turn, these densities determine the sheath thickness and the sheath voltages $V_a$ and $V_b$.

In this work, we present computational results obtained using spherical and cylindrical many-particle simulation models which we compare with theoretical results. The simulation codes[3] are PDC1 (cylindrical) and PDS1 (spherical) which utilize particle-in-cell techniques plus Monte-Carlo simulation of electron-neutral (elastic, excitation and ionization) and ion-neutral (scattering and charge-exchange) collisions[4].

## II. SIMULATION PROCEDURE

PDC1 (PDS1) is a one dimensional, radial, electrostatic code simulating a plasma contained between concentric cylinders (spheres) coupled to an external RLC circuit and an RF source, as shown in Figure 1. Particles of finite thickness, cylindrical shells in PDC1 and spherical shells in PDS1, are placed in a gridded system, and weighted to the grid to obtain the density $\rho_j$ at the grid

points. The grid which is mathematical, not physical, is used to solve for the fields. The particles are assumed to have uniform density, which allows us to use the area of rings and the volume of shells to weight the charges to the grids in PDC1 and PDS1 as shown in the Figure 2. The density on the grid is used to solve Poisson's equation, $\nabla^2\Phi = -\rho/\varepsilon$. Once the potentials are known, the electric field on the grid can be obtained from $E = -\nabla\Phi$. The particles are moved by obtaining $E$ at each particle position using some weighting (in our case, the same used to weight particles) and applying this to the Newton-Lorentz force equation:

$$\frac{d\mathbf{v}_i}{dt} = \frac{q_i}{m_i}(\mathbf{E}(\mathbf{r}_i) + \mathbf{v}_i \times \mathbf{B})$$

The particle-in-cell method is covered in detail by Birdsall and Langdon (1985)[5].

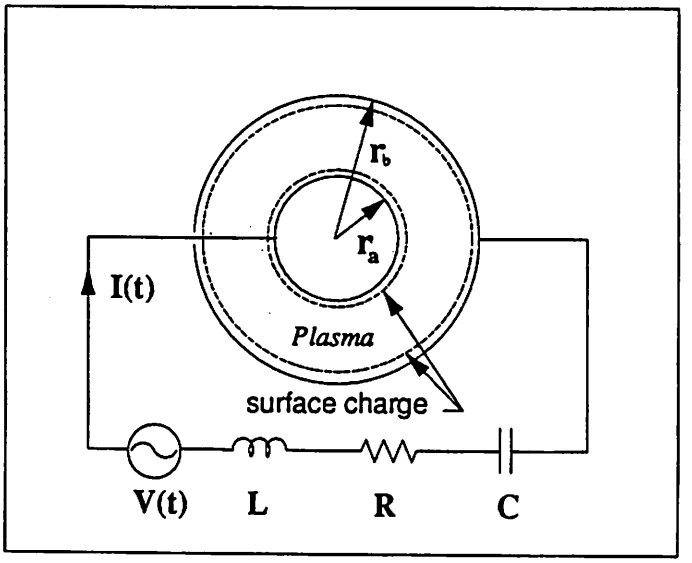


Figure 1. Cylindrical (spherical) plasma device with an external RLC circuit.

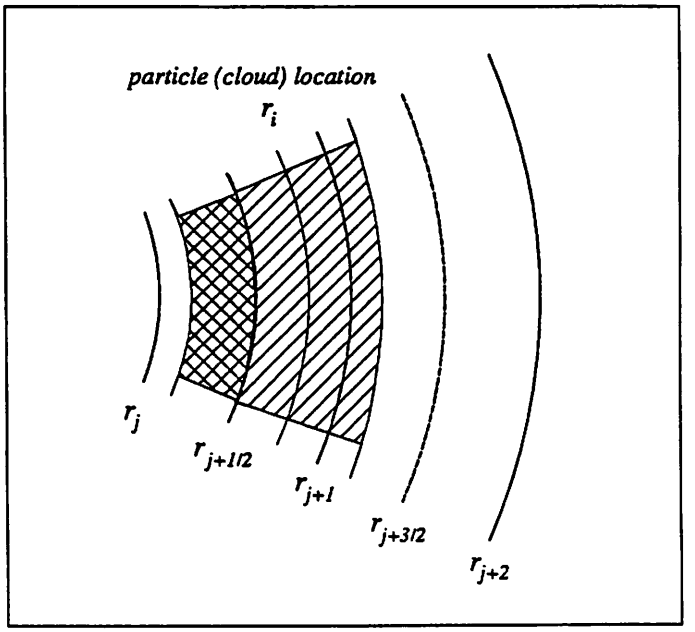


Figure 2. Particle weighting to $r_j$ grid points, using area (for cylindrical) or volume (for spherical) ratio. The particle at $r_i$ extends over two cells ($j$ and $j+1$) with the cross-hatched fraction assigned to $j$ and the slanted fraction assigned to $j+1$.

Poisson's equation is solved to obtain the potential in the plasma region. The boundary conditions are given by:

$$\oint_S \vec{E} \cdot d\vec{S} = \int_V \frac{\rho}{\varepsilon} dV + \frac{A_a \sigma_a + A_b \sigma_b}{\varepsilon} = 0$$

where the surface $S$ encloses the plasma and the boundaries and the quantities $\sigma_a$ and $\sigma_b$ refer to surface charge densities on powered and grounded electrode respectively.

Poisson's equation can be combined with the circuit equation and rearranged to obtain a self-consistent field solution matrix. PDC1 (PDS1) solves this matrix every time step to obtain the spatial potential and the subsequent circuit current self-consistently to second order accuracy[6]. The matrix can be solved using any algorithm optimized for tridiagonal matrices[7]. In order to model

weakly ionized discharges with large neutral populations, accurate models of elastic, excitation, and ionizing electron-neutral collisions and scattering and charge-exchange ion-neutral collisions are included[4].

## III. THEORETICAL MODELS

In recent years, some analytic models have been developed for the sheath voltage ratio $V_a/V_b$. A model based on probe theory, which includes the effect of the floating potential and fits some of the experiments, was developed by Pointu[8], who assumes collisionless sheaths and equal ion current densities at the electrode surfaces. A one dimensional spherical shell model[9] and a finite length cylindrical model[10] have also been developed. These models incorporate various assumptions for the sheath and glow physics, yielding scalings more in agreement with measurements. We compare our simulation results for the cylindrical and the spherical case with modified versions of these models.

We use the same notation and definitions given in reference 10. The relation between the RF voltage amplitude $\tilde{V}_{a(b)}$ and the DC voltage drop $V_{a(b)}$ is given by9:

$$\tilde{V}_{a(b)} = V_{a(b)} - V_{fa(b)} \tag{1}$$

where

$$V_{fa(b)} = \frac{T_e}{2} \ln\left(\frac{MT_e}{4\pi^2 m \tilde{V}_{a(b)}}\right) \tag{2}$$

is the floating potential and $\tilde{V}_{a(b)} \gg T_e$. Figure 3 shows a typical plot of potential versus position during an RF period and the definitions used in this work.

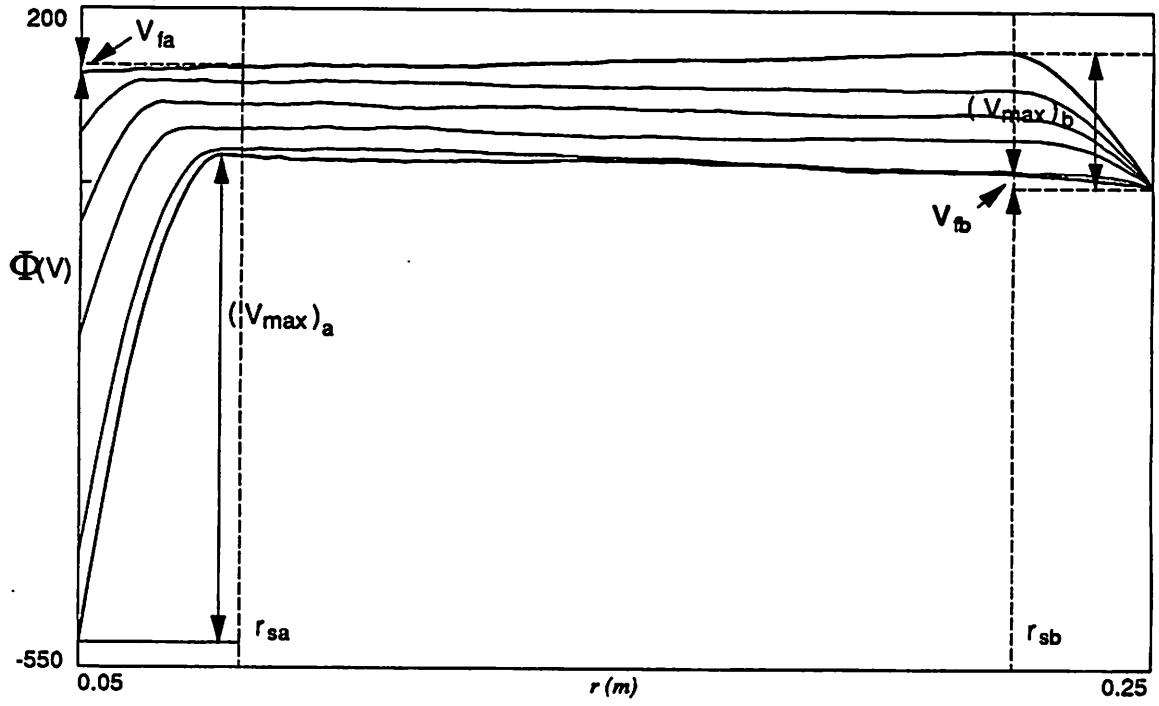


Figure 3. Typical potential during an RF period for an asymmetric discharge. This particular simulation result was obtained from PDC1 with argon as the background neutral gas at p=30 mTorr and $A_b/A_a = 5$. It shows how $V_{fa(b)}$ and $V_{a(b)} = ((V_{max})_{a(b)} - V_{fa(b)})/2$ are measured.

For high voltage capacitive sheaths, $\tilde{V}_{fa(b)} \ll V_a$ and $\tilde{V}_a \approx V_a$. In this limit, we assume that RF current density is related to the DC sheath voltage and sheath thickness by a capacitive scaling:

$$J_{a(b)}(\bar{x}) \propto \frac{V_{a(b)}}{s_{a(b)}(\bar{x})}. \tag{3}$$

where $\bar{x}$ specifies the position on the electrode surface and the voltages are independent of $\bar{x}$[10]. The total RF current $I_b$ flowing to the powered electrode is

$$I_a \propto \int_{A_a} J_a(\bar{x}) d^2x . \tag{4}$$

The relationship between the density $n_s(\bar{x})$ at the plasma-sheath edge, the DC glow-to-electrode voltage, $V_{a(b)}$, and the sheath thickness, $s(\bar{x})$, depends on the assumptions we make for the sheath. For an ion collisionless sheath, we assume a Child's law dependence[9]

$$n_{sa(b)}(\bar{x}) \propto \frac{V_{a(b)}^{3/2}}{s_{a(b)}^{2}(\bar{x})}. \tag{5}$$

For an ion collisional resonant charge transfer sheath, we assume that[9]

$$n_{sa(b)}(\bar{x}) \propto \frac{V_{a(b)}^{3/2}}{s_{a(b)}^{5/2}(\bar{x})}. \tag{6}$$

For an ion collisional elastic scattering sheath we assume that [11]

$$n_{sa(b)}(\bar{x}) \propto \frac{V_{a(b)}^{2}}{s_{a(b)}^{3}(\bar{x})}. \tag{7}$$

Using equations (3), (4) and the various sheath models above, we obtain[10]:

$$\frac{V_a}{V_b} = \left(\frac{1 - V_{fb}/V_b}{1 - V_{fa}/V_a}\right)^q \left(\frac{V_a}{V_b}\right)_0, \tag{8}$$

where

$$\left(\frac{V_a}{V_b}\right)_0 = \left(\frac{\int_{A_b} n_{sb}^p(\bar{x}) d^2x}{\int_{A_a} n_{sa}^p(\bar{x}) d^2x}\right)^q. \tag{9}$$

$V_a$ and $V_b$ are related to the peak-to-peak voltage $\tilde{V}_{pp}$, appearing at the target electrode, by

$$V_a + V_b = V_{fa} + V_{fb} + \tilde{V}_{pp}/2 \tag{10}$$

and $p$ and $q$ depend on the sheath model, as shown in Table 1.

For most simulation parameters, our results indicate that the ionization rate is highest near the sheaths; e.g., in the cylindrical case shown in Figure 4b. This local ionization is due to stochastic electron heating produced by the oscillating sheaths and occurs when the mean free path for

ionization by electrons is smaller than the discharge length. Figure 4a shows the electron charge density across the system, averaged over an RF period, $q\overline{n_e}$. The number of ionizations occurring in a grid cell per time interval is given by $\overline{n_e}\nu_{iz}V_j$ where $V_j$ is the cell volume and $\nu_{iz}$ is the ionization rate shown in Figure 4b; this rate is obtained cumulatively, over the entire run.

Assuming that local ionization near each sheath dominates the overall ionization, we obtain the scaling[9]

$$\frac{n_{sa}}{n_{sb}} = \frac{V_a}{V_b}. \tag{11}$$

Using (11) in (9) we obtain:

$$\left(\frac{V_a}{V_b}\right)_0 = \left(\frac{A_b}{A_a}\right)^{\frac{q}{1+p+q}} \tag{12}$$

Table 1 shows the values for $p$, $q$ and the exponent in equation (12), $q/(1+p+q)$ for the various sheath models.

Table 1. Exponents for various sheath scaling laws and for the zero order relationship between the sheath voltage ratio and area ratio.

| Sheath Ion Model | $p$ | $q$ | $\frac{q}{1+p+q}$ |
|---|---|---|---|
| Collisionless | 1/2 | 4 | 8/11 (0.7273) |
| Elastic Scattering | 1/3 | 3 | 9/13 (0.6923) |
| Resonant Charge Exchange | 2/5 | 5/2 | 25/39 (0.641) |

Solving (8), (10) and (12) numerically, we obtain the values for $V_a/V_b$ in terms of $A_b/A_a$. Observe that there is a dependence of $V_a/V_b$ on the electron temperature, $T_e$, due to the dependence of the floating potential on $T_e$.

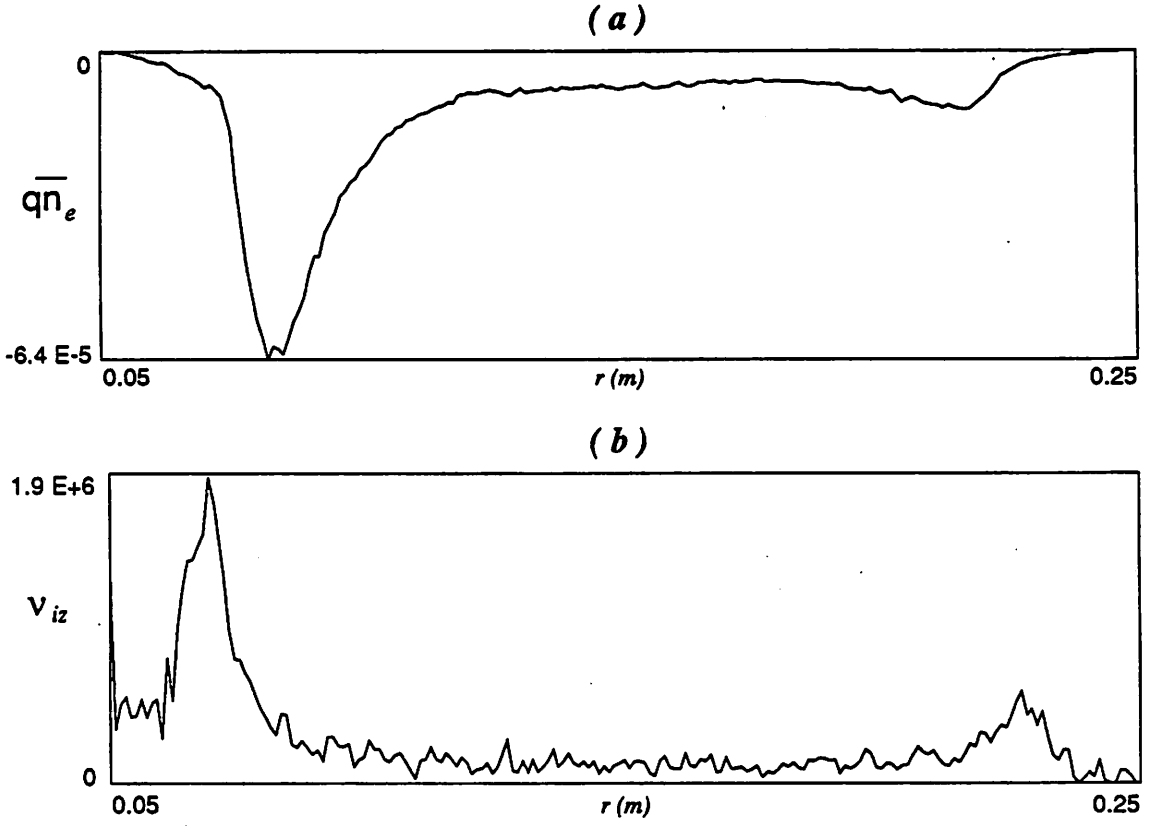


Figure 4. (a) Typical spatial variation of the charge electron density averaged over an RF period and (b) the ionization rate, $\nu_{iz}$, in the cylindrical system (cumulative in time). These results were obtained from PDC1 with argon (collisional ions) as the background neutral gas at p = 30 mTorr and $A_b/A_a = 5$.

## IV. SIMULATION RESULTS FOR VOLTAGE RATIOS

Several runs were done using PDC1 and PDS1 for different area ratios, two kinds of background gas (hydrogen and argon), and with and without ion-neutral collisions. The area ratio, defined as $A_b/A_a$, varies from 1.3 to 15. The inner and outer radius were chosen to maintain the same plasma length $l$ where $l = r_b - r_a$ (20 cm) for different area ratios. The external capacitance was chosen so that the blocking capacitor has negligible impedance at the RF driving frequency compared to the vacuum capacitance of the discharge.

Figure 3 for argon and Figure 5 for hydrogen show typical potentials, $\Phi$, across the bounded region as a function of position, at different times during an RF period, for cylindrical and spherical models. In the simulation, the potential at the outer electrode is always set to zero (reference potential). In the figures, "collisionless ions" and "ion-neutral collisions" mean that ion-neutral collisions in the simulations are turned off or turned on, respectively, across the system. Electron-neutral scattering, excitation and ionization are always present. The plasma characteristics will determine the collisionality regime in the sheath.

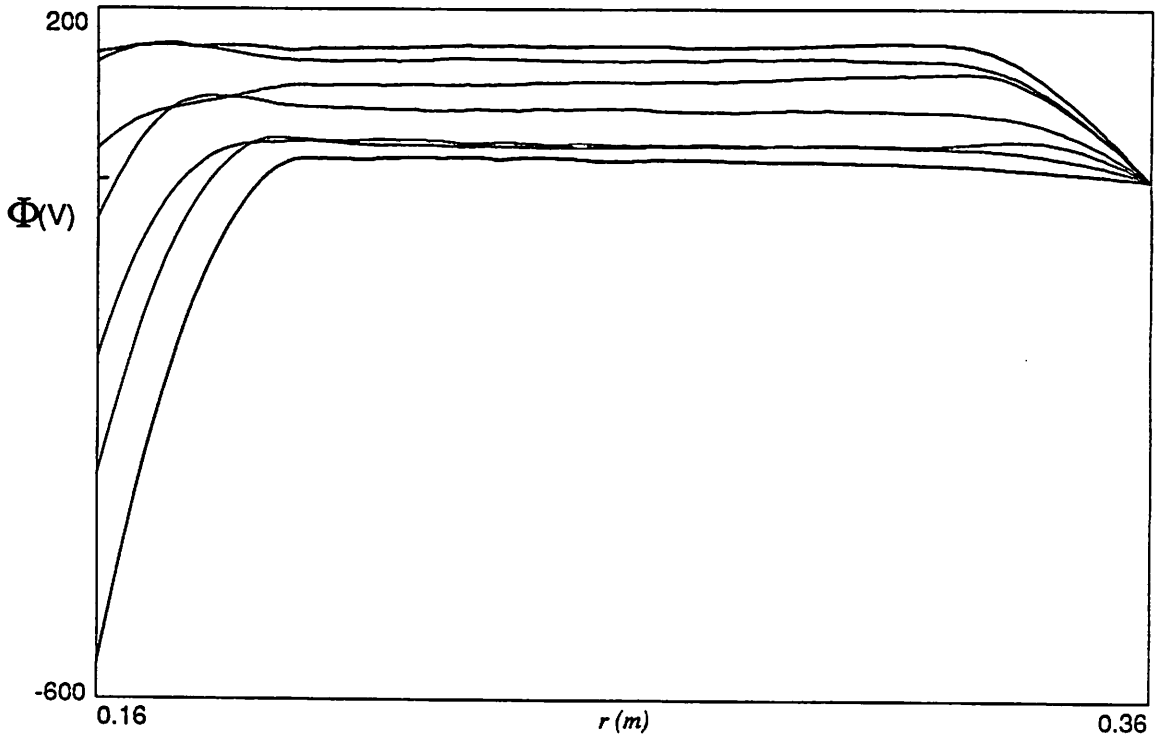


Figure 5. Potential across the system during an RF period obtained from PDS1 with hydrogen (collisional ions) as the background neutral gas at p=30 mTorr and $A_b/A_a = 5$.

The potentials $V_{a(b)}$ are referenced to the plasma potential by $V_{a(b)} = \Phi_{a(b)} - \Phi_p$ , obtained as shown in Figure 3. We assume that $V_{a(b)}$ is given by half the difference between the electrode-plasma voltage at times equal to $T/4$ and $3T/4$, for the applied Rf voltage $\propto \sin \omega_0 t$. The peak-to-peak voltage, $V_{pp}$, is obtained using equation (10). The floating potential is the difference between the potential at the electrode, *a* or *b*, and the potential at the plasma sheath edge, indicated in Figure 3 by $r_{sa(b)}$, at times equal to $3T/4$ and $T/4$ respectively.

Figures 6 and 7 show the simulation and the analytic results for cylindrical electrodes for $V_a/V_b$ versus $A_b/A_a$ for hydrogen and argon. The analytic points were obtained by solving Equations (8), (10) and (12) numerically, assuming a collisionless sheath and using the electron temperature and

the peak-to-peak potential given by the simulations. We observe that the best fit for the points, shown in Figures 6 and 7, is somewhat different from Equation (12) and the exponent in Table 1. The discrepancy may be due to the inclusion of the floating potential (not included in equation (12)) in numerical calculations. We also observe that the difference introduced by the floating potential is more noticeable for argon then for hydrogen, since the electron temperature is higher for argon. Typically $T_e \approx 0.4$~$0.6$ eV in hydrogen and $T_e \approx 2$~$3$ eV in argon.

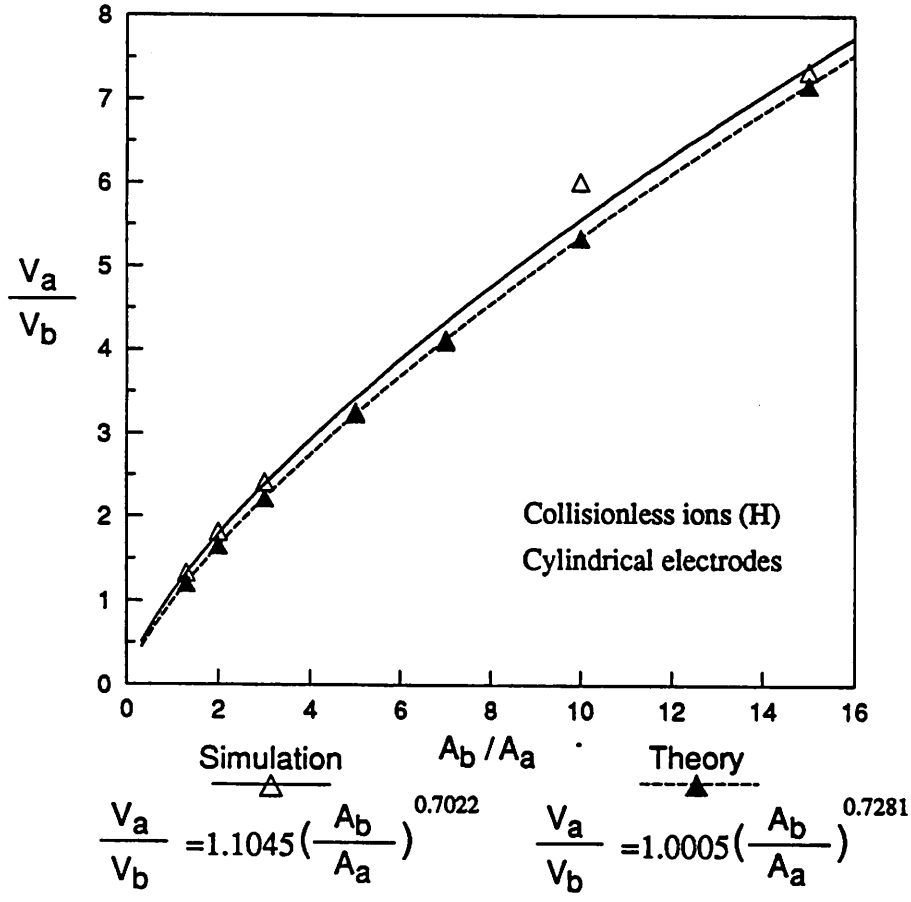


Figure 6. $V_a/V_b$ versus $A_b/A_a$ for hydrogen gas at 30 mTorr (collisionless ions in the simulation and the theory assumes a collisionless sheath model). The equations are the best fits to the data.

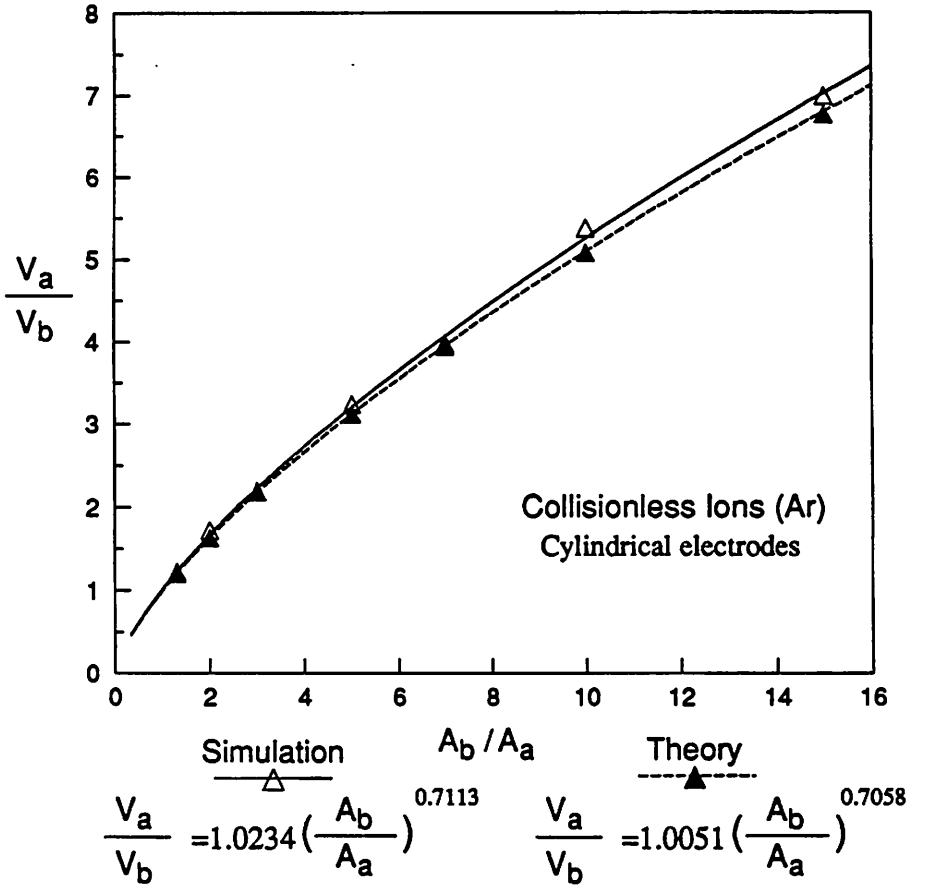


Figure 7. $V_a/V_b$ versus $A_b/A_a$ for argon gas at 30 mTorr (collisionless ions in the simulation and the theory assumes a collisionless sheath model).

Figure 8 shows the results for hydrogen, including ion-neutral collisions in the simulation, for cylindrical electrodes. We can see that, even in this case, the best agreement, looking just the numerical values, is given by the theoretical points obtained assuming a collisionless ion sheath model even though the inner electrode sheath thicknesses measured in the simulations are quite a few mean free paths for ion-neutral collisions: $s_a \approx 10 \sim 15\lambda_i$. We also can observe that if we do not include the multiplicative factor involving the floating potentials in equation (8), the best fit is

given by the collisional scattering sheath model (the exponents are the same for simulation and theory). The reason for that may be the fact that we assume in our model $\bar{V}_{fa(b)} \ll V_a$, which is not always observed in the simulations.

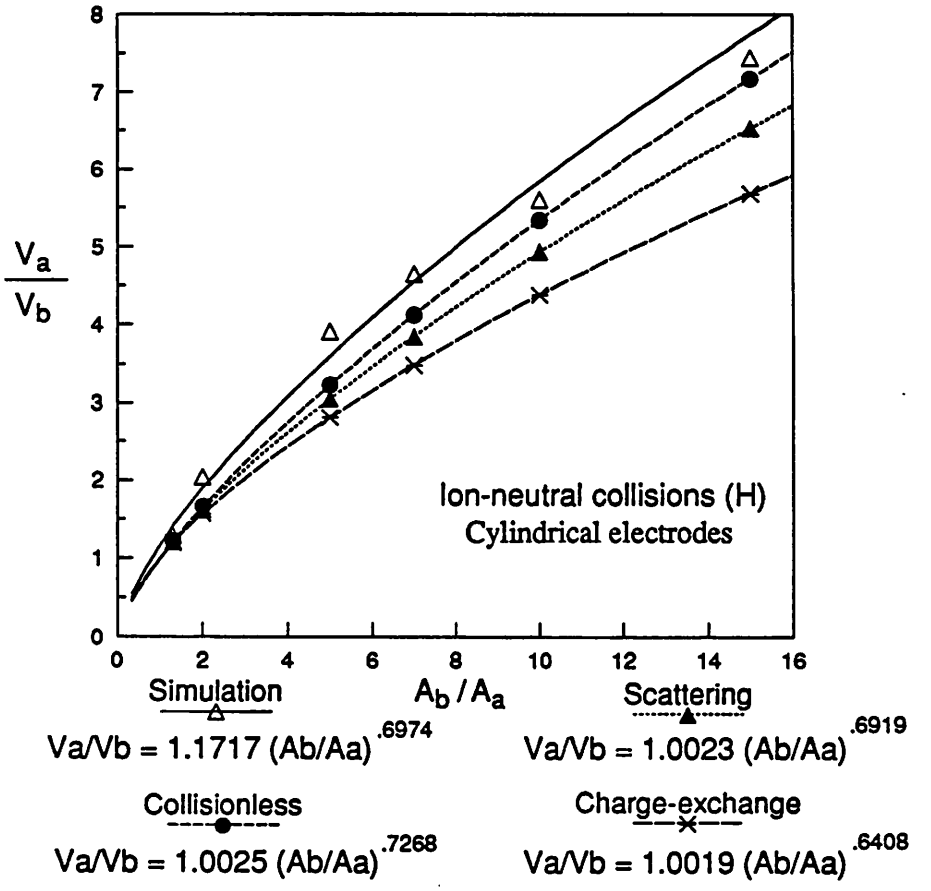


Figure 8. $V_a/V_b$ versus $A_b/A_a$ for hydrogen gas at 30 mTorr (ion-neutral collisions in the simulation). The theoretical points were obtained assuming the different models for the sheath, as indicated.

The computer runs were done using an applied potential of 500 V, RF frequency of $1 \times 10^7$ Hertz and pressure of 30 mTorr. In the simulation, the pressure and the neutral temperature (in all runs considered as the room temperature) are used to determine the neutral density which is then

used to determine the collision probability of a given particle. The neutral density is considered constant and uniform in space. The final electron temperature depends on the gas and also on the pressure used.

Note that the derivation of Equation (12) does not consider any particular electrode shape, if we consider $s_a \ll r_a$. However, simulations using spherical electrodes done using the same general parameters ( electrode separation, pressure and background gas) do not show the same agreement with theory for large area ratios as for cylindrical electrodes. We still observe a localized ionization close to the powered electrode, as shown in Figure 9, but the local ionization relationship (11), between densities at the sheaths and voltages, is no longer verified. Figure 10 shows $(n_a V_b)/(n_b V_a)$ versus area ratio for cylindrical and spherical electrodes. We observe that for cylindrical electrodes $(n_a V_b)/(n_b V_a)$ is very close to one, as expected from equation (11), up to an area ratio of 10. However, for spherical electrodes, the local ionization relation breaks down for area ratios greater than about 3.

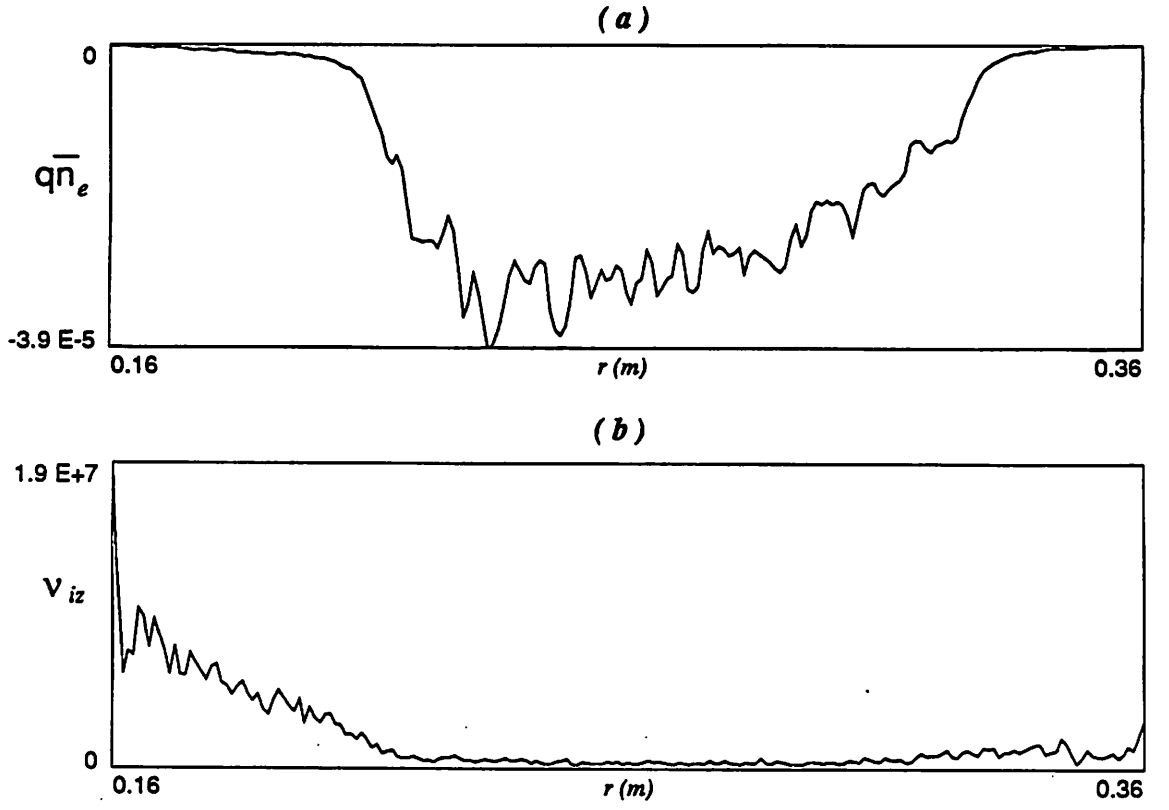


Figure 9. (a) Typical spatial variation of the electron charge density averaged over an RF period and (b) the ionization rate, $\nu_{iz}$, with spherical electrodes (cumulative in time), $A_b/A_a > 3$. In this particular result the background neutral gas was hydrogen (collisionless ions) at p=30 mTorr and $A_b/A_a = 5$.

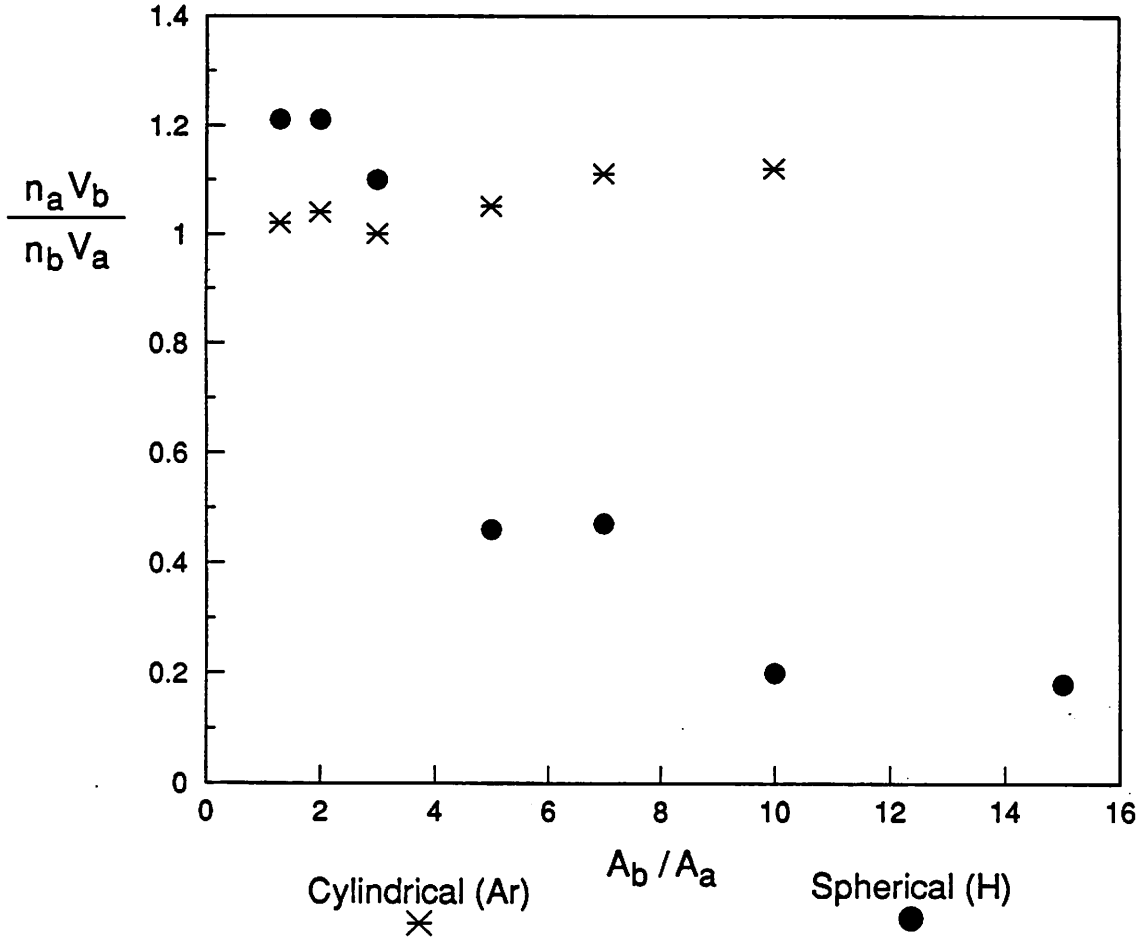


Figure 10. $(n_a V_b)/(n_b V_a)$ versus $A_b/A_a$, for cylindrical and spherical electrodes.

Hence, the discrepancy in the scaling of $V_a/V_b$ with area ratio observed for spherical electrodes is due to the very small peak in ionization rate seen at the outer electrode; i.e. the local ionization model is no longer valid, and the density $n_{sb}$ at the outer electrode may be determined by diffusion of plasma generated near the inner electrode, and not by ionization due to local stochastic heating at the outer electrode. For small area ratios, $A_b/A_a < 3$, the relationship (11) is nearly verified and we observe reasonable comparison between the simulation and the theoretical results, obtained assuming a collisionless sheath, in the Figures 11 and 12.

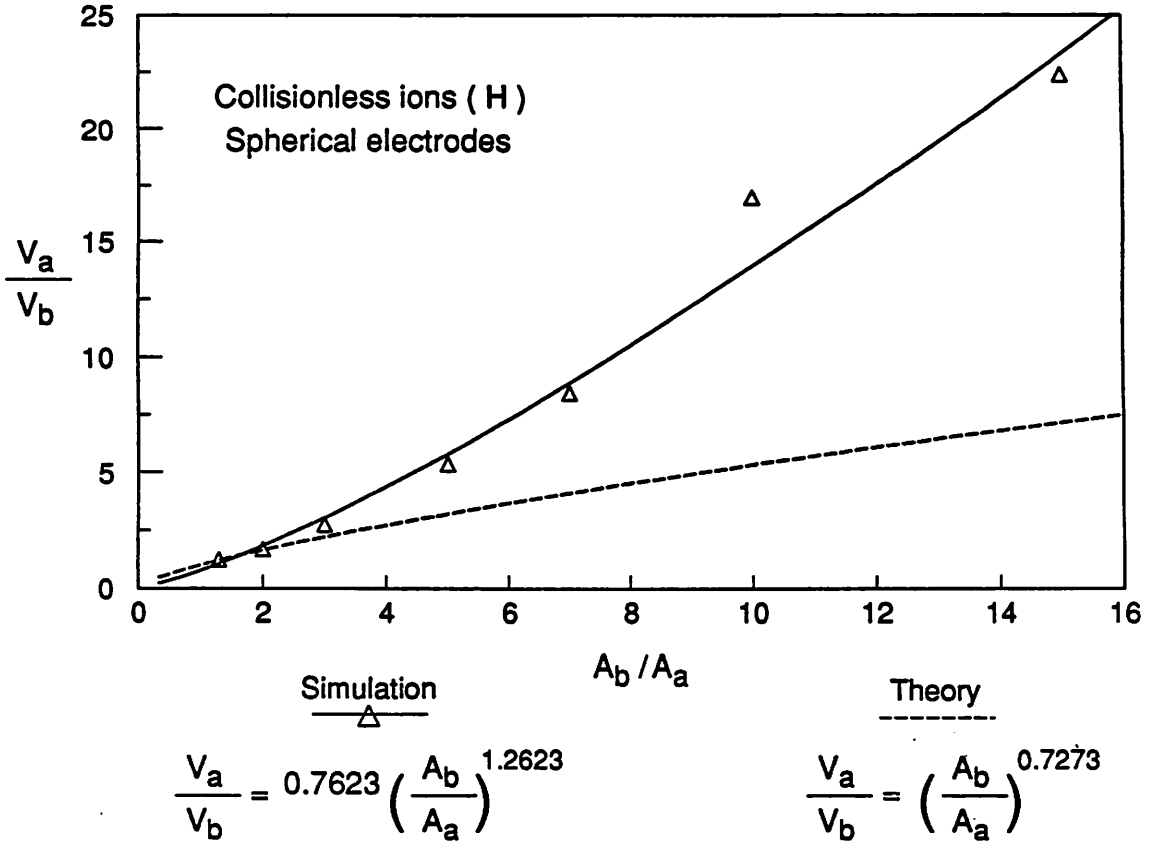


Figure 11. $V_a/V_b$ versus $A_b/A_a$ for hydrogen gas (collisionless ions in the simulation), with spherical electrodes.

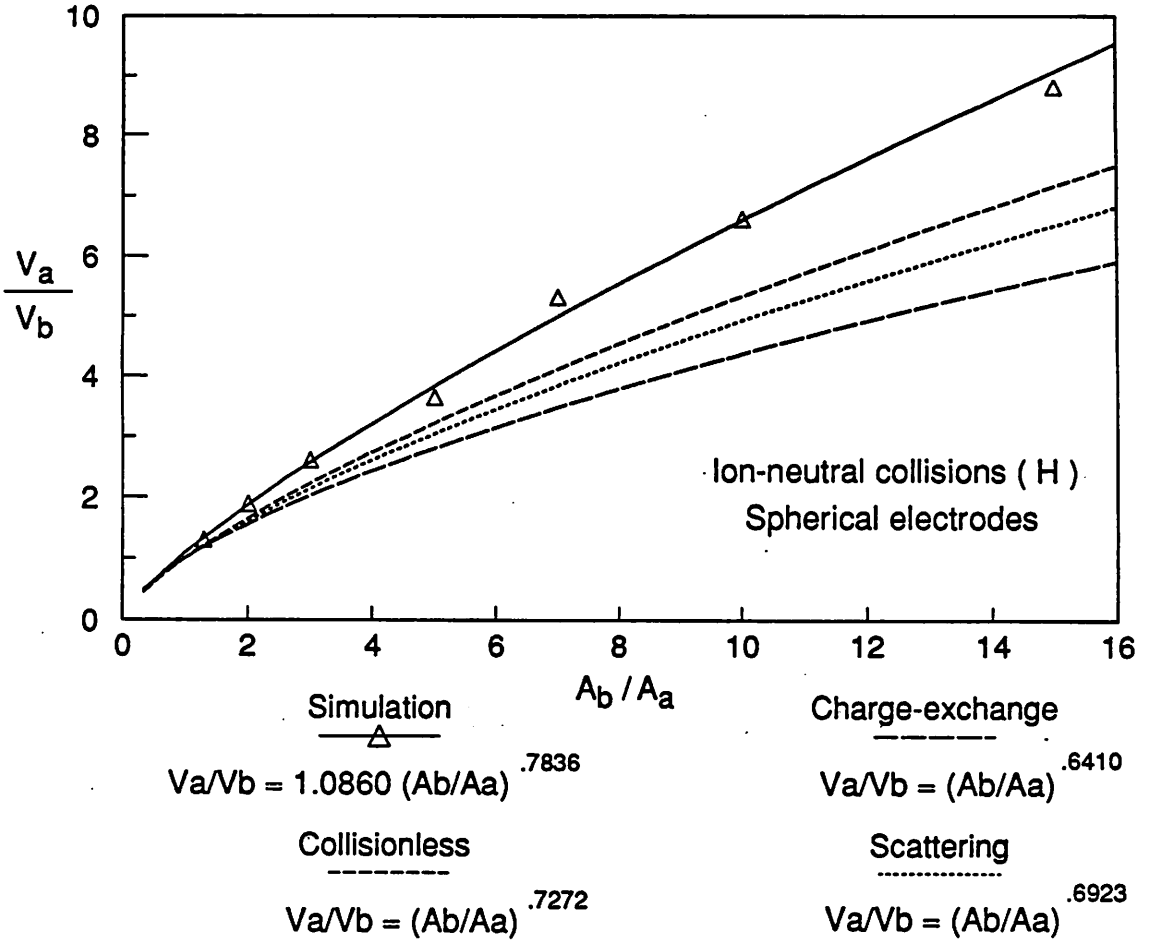


Figure 12. $V_a/V_b$ versus $A_b/A_a$ for hydrogen gas (ion-neutral collisions in the simulation), with spherical electrodes.

## V. SIMULATION RESULTS FOR BIAS VOLTAGE RATIOS

The quantity measured in most experiments is the "bias ratio", defined as the bias voltage $V_{bias} = -(V_a + V_b)$, normalized to the peak-to-peak RF voltage, $V_{pp}$. Hence, we present simulation results for this ratio, to be used for comparison with experiments. Figures 13-15 show the simulation results for bias ratio versus inverse area ratio, for all the runs. Although we have conditions differing from experimental bias measurement results (the electrode shapes are different and the final electron

temperature in the simulation is lower then in the experiments, which results in a negative floating potential), we observe that our results are in the same range of magnitude as typical experimental results; e.g., see Reference 10.

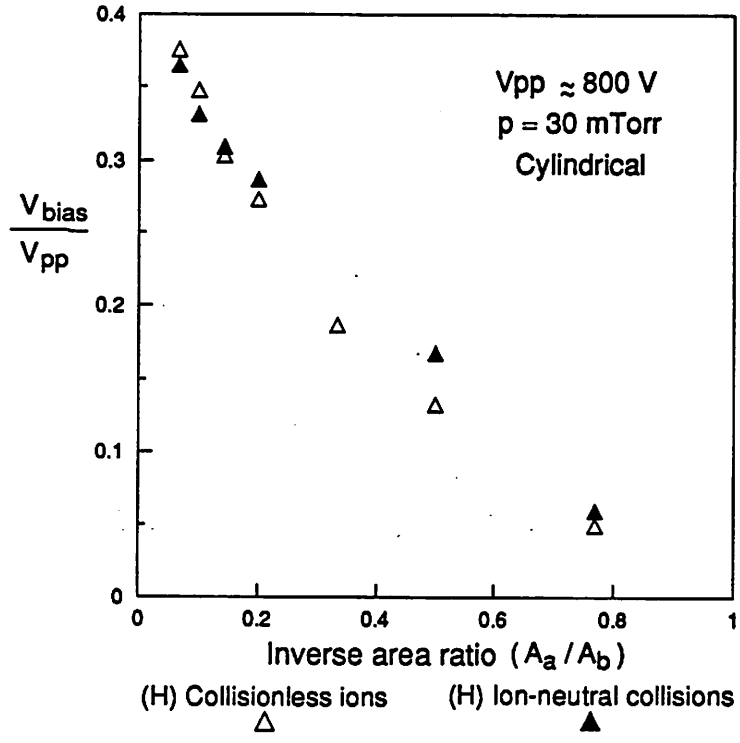


Figure 13. $V_{bias}$ versus $A_a/A_b$ for hydrogen gas (collisionless ions and ion-neutral collisions in the simulation), with cylindrical electrodes.

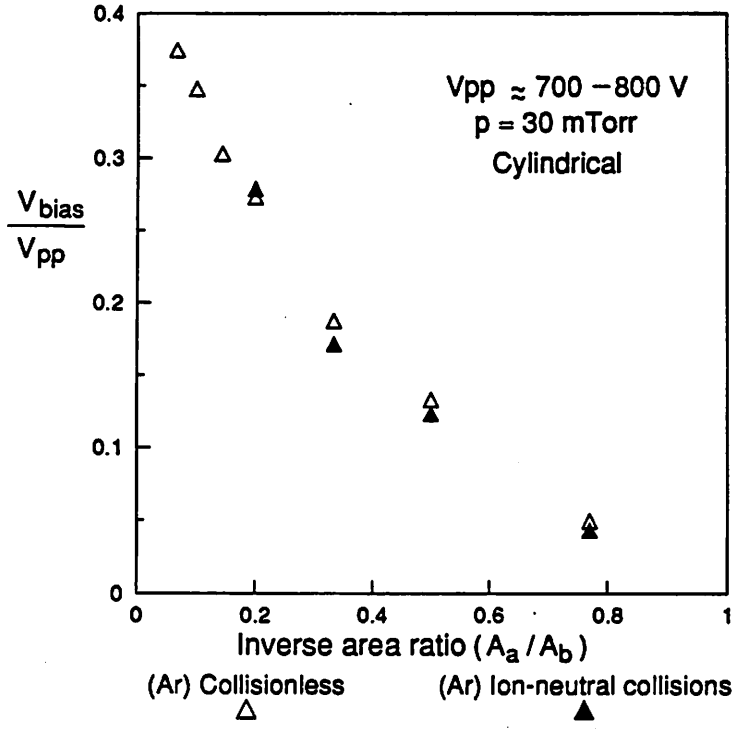


Figure 14. $V_{bias}$ versus $A_a/A_b$ for argon gas (collisionless ions and ion-neutral collisions in the simulation), with cylindrical electrodes.

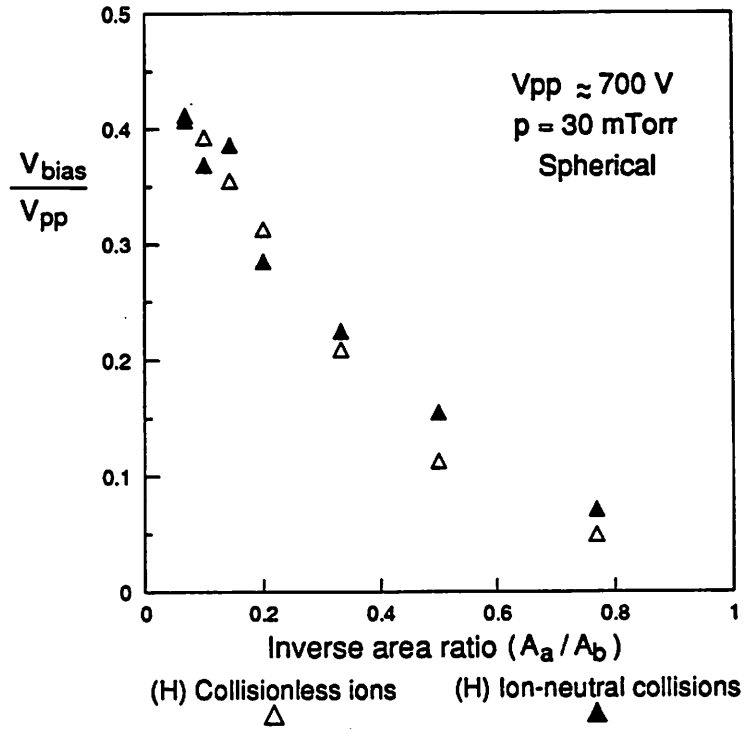


Figure 15. $V_{bias}$ versus $A_a/A_b$ for hydrogen gas (collisionless ions and ion-neutral collisions in the simulation), with spherical electrodes.

## VI. CONCLUSIONS

The relationship between the voltage ratio and area ratio in asymmetric RF discharges has been studied using spherical and cylindrical many-particle models and two different background gases at a single pressure of 30 mTorr. Over a limited range of area ratios it was found that the power dependence was close to one, not four as a collisionless uniform ionization discharge model predicts. A local ionization model is in good agreement with the simulations for those area ratios where local ionization was observed in the simulations. The transition to a nonlocal model must be studied analytically in order to compare the simulations with an analytical model in this regime. We observe that the simulation results agree very well with theory for small area ratio, $A_b/A_a < 3$, independent

of the geometry used. The model used for the sheath in this range does not play a very important role (see Figures 9 and 13). Additional simulations at pressures both above and below 30 mTorr are needed in order to test the validity of the analytic model.

## ACKNOWLEDGMENTS

This work is supported in part by ONR contract N00014-90-J-1198, NSF Grant ECS-8517363 and DOE Grant DE-FG03-87ER13727.
M. V. Alves supported partially by CAPES-Ministry of Education, Brazil

## REFERENCES


1. B. Chapman, *Glow Discharge Processes-Sputtering and Plasma Etching*, John Wiley & Sons (1980)
2. C. M. Horwitz, *J. Vac. Sci. Technol. A*, **1**:60, (1983); K. Kohler, J.W. Coburn, D. E. Horne, E. Kay and J.H. Keller, *J. Appl. Phys.*, **57**:59, (1985)
3. Codes available from Industrial Liaison Program, EECS Dept., UC Berkeley.
4. M. V. Alves, V. Vahedi and C. K. Birdsall, *Bull. APS*, **34**:2028, (Abstract) (1989)
5. C. K. Birdsall and A. B. Langdon, *Plasma Physics Via Computer Simulation*, McGraw-Hill (1985)
6. J. P. Verboncoeur, M. V. Alves, V. Vahedi, *Simultaneous Potential and Circuit Solution for Bounded Plasma Particle Simulation Codes*, in preparation.
7. W. H. Press, B. P. Flannery, S. A. Teukolsky, W. T. Vetterling, *Numerical Recipes in C - The Art of Scientific Computing*, Cambridge University Press (1988)
8. A. M. Pointu, *Appl. Phys. Lett.*, **50**:1047 (1987)
9. M. A. Lieberman, *J. Appl. Phys.*, **65**:4186 (1989)
10. M. A. Lieberman and S. E. Savas, to appear in *J. Vac. Sci. Technol. A*, (1990)
11. J. D. Cobine, *Gaseous Conductors* (Dover, New York,1941), p.128.